ChemPubSoc Europe

DOI: 10.1002/chem.201402707

CHEMISTRY A European Journal Full Paper

Gold Nanoparticles

Effect of Gold Nanoparticles on the Structure and Electron-Transfer Characteristics of Glucose Oxidase Redox Polyelectrolyte-Surfactant Complexes

M. Lorena Cortez,[a, b] Waldemar Marmisollé,[a] Diego Pallarola,[b] Lía I. Pietrasanta,[c] Daniel H. Murgida,[a] Marcelo Ceolín,[b] Omar Azzaroni,*[b] and Fernando Battaglini*[a]

Abstract: Efficient electrical communication between redox proteins and electrodes is a critical issue in the operation and development of amperometric biosensors. The present study explores the advantages of a nanostructured redox-active polyelectrolyte–surfactant complex containing $[Os(bpy)_2Clpy]^{2+}$ (bpy = 2,2′-bipyridine, py = pyridine) as the redox centers and gold nanoparticles (AuNPs) as nanodomains for boosting the electron-transfer propagation throughout the assembled film in the presence of glucose oxidase (GOx). Film structure was characterized by grazing-incidence small-angle X-ray scattering (GISAXS) and atomic force microscopy (AFM), GOx incorporation was followed by surface plasmon resonance (SPR) and quartz-crystal microbalance with dissipation (QCM-D), whereas Raman spectroelectrochemistry and electrochemical studies confirmed the ability of the entrapped gold nanoparticles to enhance the electron-transfer processes between the enzyme and the electrode surface. Our results show that nanocomposite films exhibit five-fold increase in current response to glucose compared with analogous supramolecular AuNP-free films. The introduction of colloidal gold promotes drastic mesostructural changes in the film, which in turn leads to a rigid, amorphous interfacial architecture where nanoparticles, redox centers, and GOx remain in close proximity, thus improving the electron-transfer process.

Introduction

The development of novel materials and methods aiming to improve the sensitivity, selectivity, reliability, and time response of biosensors has placed these devices in the center of the analytical scene. Within this context, amperometric sensors are quite appealing as they can fulfill those requirements[1] with the additional potential to enable miniaturization, a fundamental requisite for implantable medical devices.[2] A key issue in the development of any biosensor is its sensitivity, which in the case of amperometric biosensors is controlled by several factors, such as substrate diffusion, redox mediator features, and the electrical communication between the recognition element and the other device components. The most studied example is the glucose biosensor, where the efficient electrical communication between the biological recognition element (GOx) and the transducer (the mediator/working electrode interface) is often challenged by the enzyme's insulating shell of amino acids. To overcome this limitation, a wide variety of surface-functionalization strategies, such as self-assembled monolayers,[3] polymers,[4] proteic coatings,[5] and hydrogels,[6] have been explored to preserve the native structure and function of the incorporated enzyme.[7]

In the past several years, carbon nanotubes[8] (CNTs) and gold nanoparticles[9] (AuNPs) have shown excellent electrocatalytic properties, which were immediately applied to the development of biosensors.[10] Particularly, the inclusion of AuNPs was intended to allow direct electron transfer, in which the electrons can directly tunnel from the catalytic center of the enzyme to the surface of the current collector,[11] even though this strategy presents some limitations.[12] Another approach is to use them as catalytic domains in the layer-by-layer (LbL) assembly of polyelectrolyte multilayers to create composite films at electrode interfaces.[13] As an alternative,[14] polyelectrolyte–surfactant complexes[15] display similar characteristics regarding surface functionalization while, at the same time, exhibiting certain benefits concerning the initial modification of the electrode surface.[16] In recent years, we have begun a systematic

[a] Dr. M. L. Cortez, Dr. W. Marmisollé, Dr. D. H. Murgida, Dr. F. Battaglini
INQUIMAE - Departamento de Química Inorgánica Analítica y Química Física, Facultad de Ciencias Exactas y Naturales
Universidad de Buenos Aires, CONICET
Ciudad Universitaria, Pabellón 2
C1428EHA Buenos Aires (Argentina)
E-mail: battagli@qi.fcen.uba.ar

[b] Dr. M. L. Cortez, Dr. D. Pallarola, Dr. M. Ceolín, Dr. O. Azzaroni
Instituto de Investigaciones Fisicoquímicas Tas y Aplicadas (INIFTA)
Departamento de Química, Facultad de Ciencias Exactas
Universidad Nacional de La Plata, CONICET
CC 16 Suc. 4 (1900) La Plata (Argentina)
E-mail: azzaroni@inifta.unlp.edu.ar

[c] Dr. L. I. Pietrasanta
Centro de Microscopías Avanzadas and Departamento de Física
Facultad de Ciencias Exactas y Naturales, Universidad de Buenos Aires
Ciudad Universitaria, Pabellón 1
C1428EHA Buenos Aires (Argentina)

approach modifying a polyallylamine-dodecyl sulfate complex (PA-DS) to introduce new functionalities to its structure,[17,18] the introduction of nanoparticles to the polyelectrolyte-complex suspension yielded remarkable electrocatalytic properties to the resulting composite material.[19]

In this report, we present studies on the functionalization of gold electrodes with AuNPs embedded in a redox-active polyelectrolyte-surfactant scaffold (OsPA-DS). The effect of the metal nanoparticles was studied by different techniques, such as resonance Raman (RR) spectroelectrochemistry, quartz-crystal microbalance with dissipation (QCM-D), surface plasmon resonance (SPR), cyclic voltammetry, grazing-incidence small-angle X-ray scattering (GISAXS), and atomic force microscopy (AFM). Our results show a significant enhancement in the electron-transfer properties of the redox centers present within the film as well as a marked effect on the catalytic behavior of GOx, where the amperometric response increases by up to five times in the presence of AuNPs. This improvement in the response is discussed in terms of the effects that AuNPs introduce to the film structure, namely electron transport through the film, mass of GOx adsorbed, stiffness/viscosity of the film, and its effect on the interaction between GOx and the osmium redox centers present in the polyelectrolyte coating. The results presented here indicate that the achieved nanoarchitecture in the presence of AuNPs allows GOx to favorably orientate within the redox network, thus providing a suitable environment to display its enzymatic potential.

Results and Discussion

The introduction of AuNPs into self-assembled systems to improve electron transfer has been widely studied;[20] and the OsPA-DS complex, containing $[Os(bpy)_2Clpy]^{2+}$ (bpy = 2,2′-bipyridine, py = pyridine), has already shown good current propagation, even in relatively thick films, and an excellent response as a mediator in enzyme catalysis.[17] Here, we have employed RR spectroelectrochemistry to assess the electrochemical connectivity of OsPA-DS films with and without the addition of AuNPs. Raman measurements were performed under resonance with the characteristic metal-to-ligand charge transfer (MLCT) electronic transition of Os^{II}, by employing 514 nm laser excitation. Under these conditions, the high-frequency region of the RR spectrum (ca. 1100–1600 cm^{-1}) is largely dominated by five bands assigned to vibrational modes of the pyridyl ligands, band that vanish upon metal oxidation, concomitant with the disappearance of the visible Os^{II} MLCT absorption band.[21] Therefore, Os^{II}/Os^{III} speciation can be easily accomplished by monitoring the potential dependence of the RR bands.

Spectra obtained for a relatively thick film of OsPA-DS on Au (28 $\mu C\,cm^{-2}$) recorded at an applied potential of 450 mV, which is sufficiently above the formal reduction potential of the Os^{3+}/Os^{2+} redox couple, exhibited a partial drop of intensity compared with the spectra obtained at the reducing potential of 0 mV (Figure 1a). These observations indicate that only a fraction of the osmium centers are efficiently wired to the Au substrate.

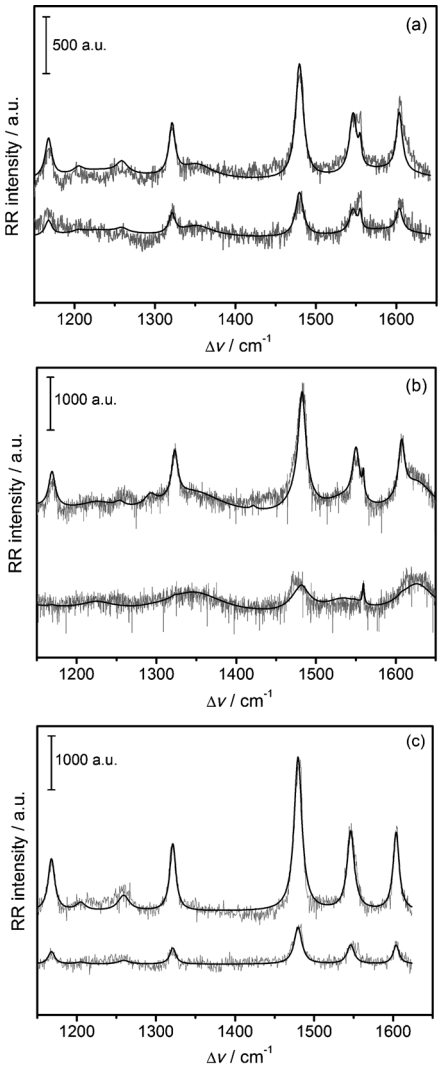

Figure 1. Resonance Raman spectra of Au electrodes coated with films of: (a) OsPA-DS; (b) OsPA-DS-AuNP (electrode **A**); (c) OsPA-DS-AuNP (electrode **B**). Upper and lower spectra in each panel were recorded at 0 V and 0.45 V applied potentials, respectively, versus Ag/AgCl.

The fraction of electroactive metal centers can be estimated as:

$$f_c = (s_0 - s_{450})/s_0 \quad (1)$$

where s_0 and s_{450} represent the integrated RR bands observed at 0 and 450 mV, respectively. The value of f_c obtained for OsPA-DS films is 0.64.

Similar experiments were carried out with two electrodes spin coated with OsPA-DS-AuNP under different conditions, resulting in voltammetric charges of 12 $\mu C\,cm^{-2}$ (electrode **A**) and 105 $\mu C\,cm^{-2}$ (electrode **B**). For the thinner film, a value of f_c very close to one was obtained, indicating that nearly 100% of the Os centers were electronically connected, whereas the significantly thicker film was characterized by $f_c = 0.80$, that is, even higher than a thin film of OsPA-DS without AuNPs. Spectra for both electrodes are presented in Figure 1b and c, re-

spectively. These results show that the intrinsically high electron connectivity of the metal centers in OsPA-DS films is significantly improved by the addition of AuNPs.

To evaluate how AuNPs can affect the GOx incorporation and catalysis in modified OsPA-DS electrodes, the adsorption process was followed by SPR and compared with blank experiments without AuNPs. Also, this technique allows electrochemical complementary tests to gain a better insight. Two gold sensors were coated with the redox-active polyelectrolyte-surfactant complex by spin coating, with and without AuNPs. The charge obtained for each electrode was similar to those obtained in the Raman experiment (Table 1). GOx was incorporated into the sensors by passing a solution of GOx (1 mg mL^{-1}) through the system, and the SPR angle shifts were converted into enzyme mass uptake as given in Table 1.

Table 1 summarizes different parameters obtained from SPR and electrochemical experiments. In the first column, the charge due to the osmium complex (Q) can be observed; using Faraday's law, the Os coverage can be calculated (column 2, Γ_{Os}). In the case of films without AuNP, a correction factor was taken into account as 36% of the redox centers are not connected. The third column corresponds to the amount of GOx adsorbed (Γ_{GOx}), and the fourth column gives the stoichiometry between the Os redox centers and GOx, showing that the incorporation of AuNP does not produce significant changes in this ratio, changes that could be considered as a disadvantage as each GOx is surrounded by a smaller number of redox centers. The fifth and sixth columns correspond to current response under glucose saturation conditions; it can be observed that even though the amount of material in the electrode with AuNPs is practically three times smaller, the catalytic currents are almost the same. This is clear evidence that the efficiency of the catalytic process is remarkably enhanced in the presence of metal NPs, where the enzymatic activity per mole of redox mediator is 3.7 times higher than in the absence of AuNPs.

To explain this behavior, we have to consider the whole reaction mechanism that takes place. Equations (2)–(4) depict a simplified mechanism for the current generation in presence of glucose:

$$Os^{II} \rightarrow Os^{III} + e^- \quad (2)$$

$$Os^{III} + GOx(FADH_2) \rightarrow Os^{II} + GOx(FAD) \quad (3)$$

$$Glucose + GOx(FAD) \rightarrow Gluconic\ acid + GOx(FADH_2) \quad (4)$$

Reaction (2) is essentially interfacial and is expected to be fast, whereas reactions (3) and (4) occur within the film. Under glucose saturation, reaction (3) can be considered the rate-determining step as no changes in the catalytic current are observed owing to glucose addition. Under these conditions, the current dependence with GOx scales with the square root of its concentration.[22] Therefore, to explain this behavior, owing to the higher coverage of GOx, this term should be more than 10 times greater in presence of AuNPs. A feasible model is to consider that when negatively charged GOx is incorporated into the film, it spontaneously occupies areas very close to the positively charged OsPA, following almost the same stoichiometric relationship in both cases. This means that the effect of AuNPs is not to increase the mass adsorption of GOx, but to produce structural changes in the film.

The structure of the film with and without AuNPs was studied by GISAXS under controlled humidity conditions (Figure 2). The aim of these experiments was to corroborate whether the presence of aqueous environments promote drastic changes in the film mesostructure owing to swelling of the polyelectrolyte domains. GISAXS characterization of OsPA-DS films shows

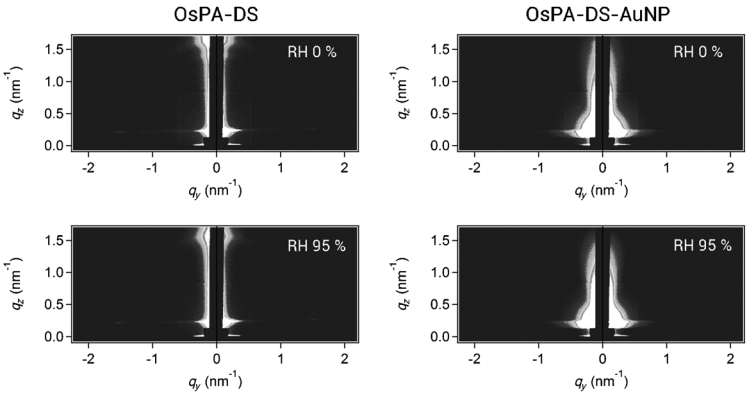

Figure 2. GISAXS patterns obtained from OsPA-DS (left) and OsPA-DS-AuNP (right) films measured at an incident angle of 0.27° under low (top) and high (bottom) humidity conditions. Films were spin-coated on Si(100) substrates.

a bright region (highest intensity) in the q_z direction (for $q_y \rightarrow 0$) (Figure 2) either in dry or humid conditions. This suggests the presence of lamellar domains oriented parallel to the substrate that remain structurally stable upon incorporation of water in the hydrophilic regions of the film. Conversely, similar experiments performed on OsPA-DS-AuNPs samples revealed that the bright spot previously observed at $q_z = 1.55$ nm^{-1} disappeared when AuNPs were incorporated into the film. On the other hand, nanocomposite films exhibit a strong scattering in the low q_z region owing to the presence of the metal nanoparticles. In a simi-

Table 1. Parameters obtained from electrochemical SPR experiments.

	Q [μCoul cm^{-2}]	Γ_{Os} [pmol cm^{-2}]	Γ_{GOx} [pmol cm^{-2}]	Γ_{Os}/Γ_{GOx}	J_{sat} [μA cm^{-2}]	j_{sat}/Γ_{Os} 10^{-3} [μA pmol^{-1}]
without AuNPs	20.8	337[a]	21.9	15.5	32.0	95
with AuNPs	8.0	83	7.2	11.5	29.0	349

[a] Considering also the "non-wired" osmium centers (36%). Q = charge due to the osmium complex, Γ_{Os} = Osmium coverage, Γ_{GOx} = GOx adsorbed, j_{sat} = current density in glucose saturation conditions.

lar way, GISAXS measurements corroborated that nanocomposite films exhibit no mesostructuring regardless of the humidity conditions (Figure 2). This observation indicates that the presence of the AuNPs strongly affects the organization of the electroactive domains within the film with a concomitant effect on the redox-active properties.

QCM-D has shown to be an efficient technique to understand structural changes in soft materials.[23] By tracking changes in frequency and dissipation it is possible to obtain information regarding mass incorporation (or loss) and changes in the viscoelastic properties of the film. Two gold-covered QCM sensors were modified with OsPA-DS with and without AuNPs. Both sensors have nearly the same density of redox centers, given that the charge density is 10.2 and 7.1 $\mu C\,cm^{-2}$, for the system without and with AuNPs, respectively.

Figure 3 shows the frequency versus time (a) and the dissipation versus time (b) variations for GOx adsorption on sensors modified with OsPA-DS (dashed line) and OsPA-DS-AuNP (solid line) nanocomposites. The strong influence of the nanoparticles in the supramolecular film on the adsorption characteristics of GOx is clear. In both cases, the initial exposure to the GOx solution leads to a rapid decrease in frequency followed by a small but steady decrease before reaching the final plateau. However, frequency changes are more pronounced for sensors modified with OsPA-DS, thus indicating that the amount of mass adsorbed on the OsPA-DS is higher.

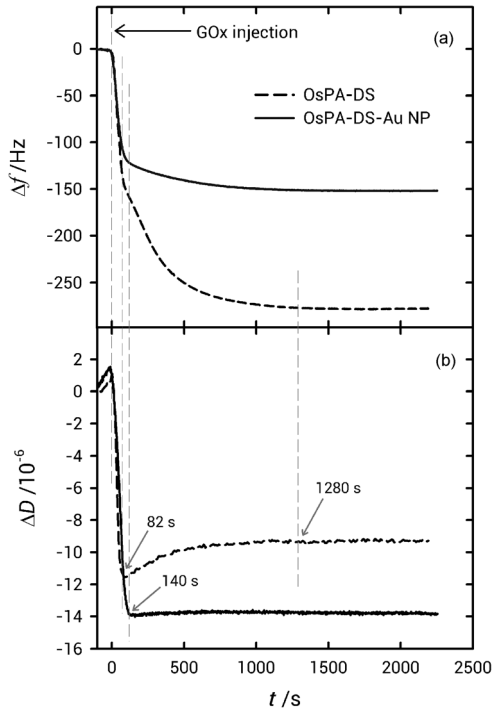

Figure 3. Changes in frequency (a) and dissipation (b) as a function of time during adsorption of glucose oxidase (GOx) onto OsPA-DS- and OsPA-DS-AuNP-modified gold-coated QCM sensors.

An interesting feature is seen when comparing the dissipation (D) trace recorded during the adsorption of GOx on both substrates. GOx adsorption on OsPA-DS shows a sharp decrease in D that is reverted at $t = 82$ s, leading to a slow steady D decrease during further adsorption of GOx. These changes in D reflect structural changes in the film upon adsorption. The decreasing D indicates that the film is changing from a soft state to a more rigid state. We hypothesize that rapid protein adsorption leads to a rather compact film that is formed during the early stages of the process. Then, gradual increase in D points to a gradual "softening" of the film during further adsorption of GOx. This effect could be attributed to considerable solvent uptake due to the GOx immobilization.

Conversely, GOx adsorption on OsPA-DS-AuNP poses a completely different scenario. The full picture of the GOx immobilization could be described by an early stage process where there is a significant increase in surface coverage. In less than 140 s, the protein layer reaches approximately 80% of the asymptotic coverage with viscoelastic characteristics that can be attributed to a rather rigid film (Figure 3b). Interestingly, in a more advanced stage (>140 s), the GOx film slowly reaches almost full (asymptotic) coverage. This lack of variation in D indicates that after initial adsorption of GOx there are no major changes in interactions at the protein/substrate interface. These experiments eloquently illustrate that the same biomolecule can form films with different viscoelastic properties depending on their interaction with the substrate.[24]

To understand such a profound difference, we performed atomic force microscopy studies in tapping mode and extension phase imaging of the morphology and heterogeneity of such films on the nanoscale prior to and after adsorption of glucose oxidase. Figure 4 illustrates the evolution of the high resolution imaging for the assemblies OsPA-DS, OsPA-DS/GOx, OsPA-DS-AuNP, and OsPA-DS-AuNP/GOx. To better illustrate the above trends, different resolution topographic images together with cross-sectional analysis and phase imaging across the same area of the sample are depicted in the same figure.

The topography images are dominated by a nanometer scale, low frequency height undulation (A, B, E, and F) that change to a more ordered structure for the assemblies containing AuNP (I, J, M, and N). Comparison of the AFM images of OsPA-DS and OsPA-DS-AuNP nanocomposites yielded interesting results (Figure 4A, B and I, J). In the case of OsPA-DS films, topographic imaging revealed the presence of aggregates with a roughness of 4.3 nm. Conversely, OsPA-DS-AuNP nanocomposites exhibited a homogeneous distribution of nanoscale bundles all over the substrate. In the latter case, the roughness of the nanocomposite film was 1.3 nm. It is evident that the presence of the metal nanoparticles plays a role in defining the morphological characteristics of the spin-coated films.

Phase imaging also showed sharp changes in the appearance of the films, providing us with information beyond topographical mapping. It revealed topographically fine features that were much less apparent in the height image (B and J) and translate to well-defined variations in phase contrast (C and K). In fact, the presence of the nanoparticles on the composite surface was readily detected during phase imaging. Although phase imaging of OsPA-DS films is featureless, similar

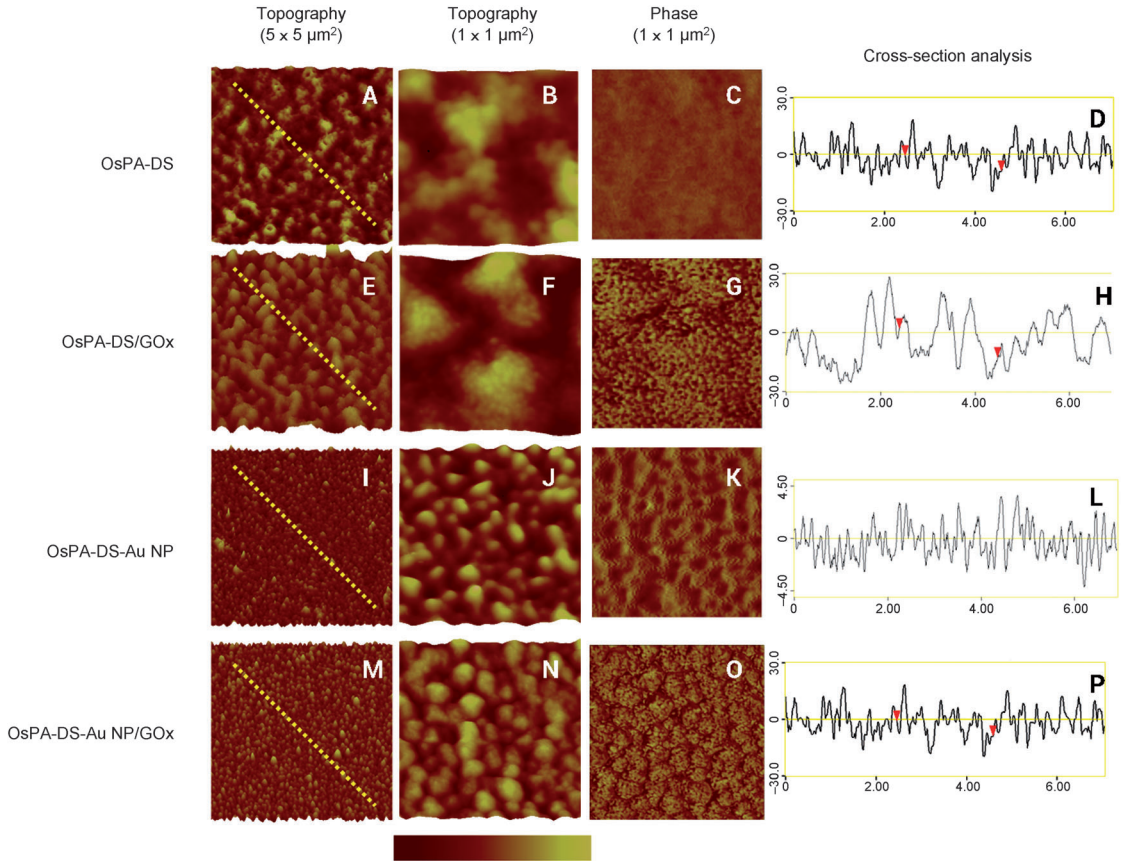

Figure 4. Topography and phase images with the corresponding cross-sectional analysis of OsPA-DS (A–D), OsPA-DS/GOx (E–H), OsPA-DS-AuNP (I–L), and OsPA-DS-AuNP/GOx (M–P). The images are presented as surface plots to emphasize features: rotation 0° and pitch 90°. Scan size 5×5 μm² or 1×1 μm², 512×512 pixels. Color represents a total range of 60 nm in the height image and 45° in the phase image.

experiments performed on OsPA-DS-AuNP nanocomposites revealed the presence of nanoparticles in the polymer film.

AFM images were also recorded after incubation of both substrates in a glucose oxidase solution. The surface morphology was strongly modified as a result of GOx adsorption. After incubation, a homogenously distributed nodular-like film is deposited on both films. However, a closer inspection of the OsPA-DS-AuNP film revealed that, in fact, enzymes are predominantly adsorbed onto the AuNPs rather than the polymeric domains. This observation is further corroborated by phase imaging of both samples after GOx adsorption (Figure 4 G and O). The appearance of fine structure in the phase images correlates with the presence of GOx. Although OsPA-DS exhibits a homogeneous distribution of bright and dark spots owing to the even distribution of GOx on the electrode surface, OsPA-DS-AuNP nanocomposites clearly indicate the presence of protein domains on top of nanoparticle aggregates. We hypothesize that the close proximity of enzymes to the AuNPs is probably the main factor that leads to the enhanced catalytic activity of the glucose oxidase. This difference may also have an important effect on the closeness of the enzyme and redox centers, and therefore in the kinetics rate of Equation (3). The enhancement effect of AuNPs on the activity of GOx itself was previously described by Chen et al.[25] They observed an enhancement of the GOx activity by adding AuNPs ranging from 10 to 30 nm in size to the enzymatic electrode. Compared with that containing the 30 nm AuNPs, the enzymatic electrode containing 10 nm particles surprisingly possessed a much higher sensitivity.[26]

In line with these results, the information obtained by SPR, QCM-D, and cyclic voltammetry reveals a much higher bioelectrocatalytic activity per mass of enzyme when AuNPs are integrated in the supramolecular nanocomposite.

To better establish the effect of AuNPs on the response to a glucose concentration range, a film was prepared under similar conditions to those used for the electrodes employed in Raman and SPR experiments to assure the maximum connectivity and comparable results, and then GOx was adsorbed. Blank experiments were prepared with the same compounds and procedures without AuNPs. The observed charge densities were 7.3 and 16.8 $\mu C\,cm^{-2}$ for the electrodes with and without AuNPs, respectively. Catalytic current in the presence of different concentrations of glucose for each electrode were determined to establish the effect of AuNPs in different step-rate scenarios (Figure 5). To more accurately compare these results, we plotted the ratio between catalytic current density at a given glucose concentration (j_{cat}) and the current density observed in absence of glucose (j_0), normalizing in this way the response to a given amount of mediator (Figure 6 a). A significant improvement in the catalytic behavior for the system con-

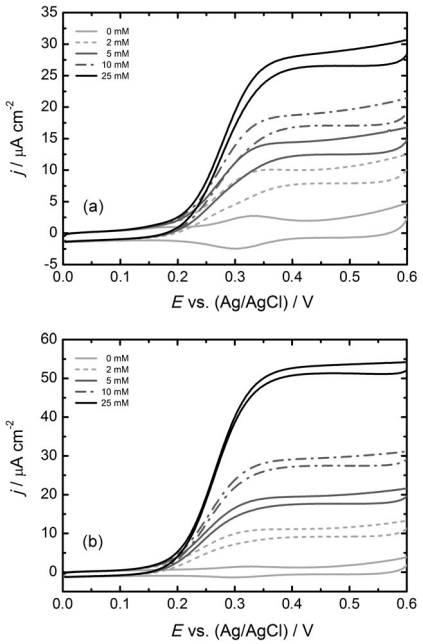

Figure 5. Bioelectrocatalytic response of composite platforms in the presence of increasing amounts of glucose: (a) Au/OsPA-DS/GOx electrode, (b) Au/OsPA-DS-AuNP/GOx electrode.

taining AuNPs is observed. Also, a striking increase in the sensitivity to glucose in the physiological concentration range is evident (Figure 6b).

The five-fold increase in the current observed at low glucose concentration and in saturated conditions means that the presence of the AuNPs has an important impact in the interaction between GOx and the metal–osmium network, thus facilitating the electron transfer process; the possible causes of this behavior are discussed below (Figure 7).

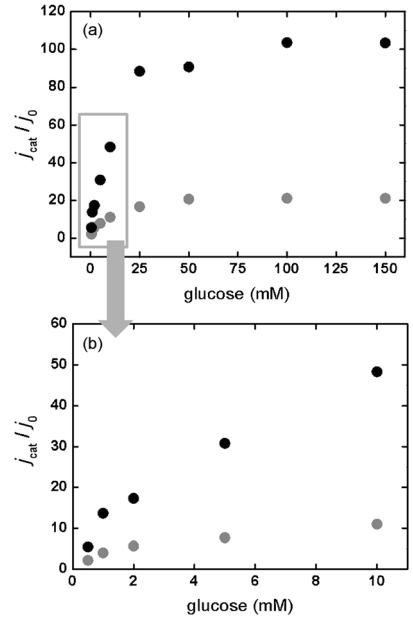

Figure 6. (a) Representation of j_{cat}/j_0 ratio as a function of glucose concentration (j_{cat} = current density observed in presence of glucose and j_0 = current density observed in absence of glucose). Black circles correspond to electrodes modified with OsPA-DS-AuNP/GOx nanocomposites; grey circles correspond to electrodes modified with OsPA-DS/GOx assemblies. (b) Detail of the response in the range between 0 and 10 mM glucose.

Conclusion

The incorporation of AuNPs into a redox-active polyelectrolyte-surfactant complex plays an important role in improving the charge propagation throughout the film and hence the electrochemical response. This effect was reflected in the ability to efficiently connect all the redox centers confined in the supramolecular thin films, and connecting 80% of the redox centers for thick films as measured by Raman spectroelectrochemistry. This behavior is in agreement with numerous works reporting the use and applications of AuNPs in electrochemical interfaces. Recently, Chazalviel and Allongue[27] have explained the improvement in the electron-transfer process on electrodes modified with organic layers decorated with AuNPs. These authors showed that the metal-to-metal electron transfer is easier than for a similar electron-transfer process between a metal surface and a redox system. This has been ascribed to the high density of states on the metal nanoparticle. This asseveration has been supported by experimental results obtained by Gooding and co-workers.[28] This model may be applied also in our work; however, the results obtained by AFM reveal profound changes in the roughness of the film with important consequences for the connections between the redox centers. In a similar vein, from a structural viewpoint, GISAXS experiments corroborated that the presence of the gold nanoparticles introduces a completely different scenario in terms of supramolecular organization. Contrary to the lamellar assemblies determined by GISAXS in the AuNP-free films (Figure 2, left), the integration of colloidal gold into the supramolecular material hinders the formation of lamellar domains and renders the nanocomposite film inner structure into an amorphous "scrambled egg" configuration (Figure 2, right); to get a clearer idea, both structures are depicted in Figure 7. We hypothesize that this disorganized "scrambled egg" configuration facilitates the intimate contact between the different counterparts within the film, including the randomly distributed AuNPs within the film.

The adsorption of GOx to the redox-active nanostructured composite provided the sensing element for glucose detection without affecting the electron-transfer rate of the Os^{3+}/Os^{2+} redox couple. GOx adsorbs tightly on both type of films and in almost the same amount per unit of polyelectrolyte complex. However, OsPA-DS led to a water-rich film, evidenced by a greater change in frequency in QCM-D experiments; whereas in OsPA-DS-AuNP, the induced structural changes due to the presence of AuNPs leads to a rather rigid assembly of GOx, as shown by dissipation and AFM experiments. This differential organization of the electroactive domains has a direct impact on the electrocatalytic behavior of the assembly.

The results shown here shed light on the effect of the mesostructure in self-assembled films and the role played by the integrated AuNPs, showing that the improvement in electron

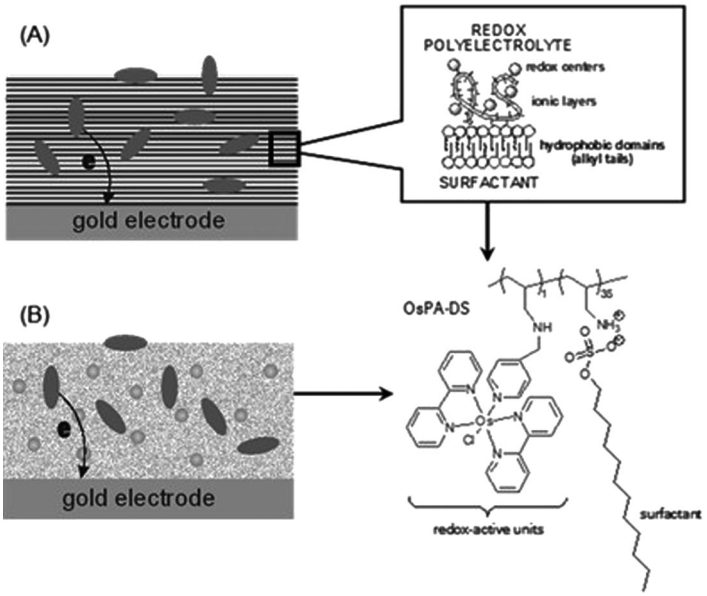

Figure 7. Simplified representation of the glucose oxidase redox polyelectrolyte-surfactant thin film assembly in the absence (a) and in the presence(b) of gold nanoparticles. The chemical structure of the different building blocks is also depicted. The lines in panel (a) represent the lamellar structure, whereas the dotted structure in panel (b) represents a "scrambled egg" configuration. Ovals represent GOx, circles AuNP.

transfer can be attributed not only to the presence of conducting metal nanoparticles, that is, high-density states,[30,31] but also to a more efficient organization of the constituting building blocks in which the redox centers and the enzyme could be constrained in a compact architecture in close proximity to the metal nanoparticles. These results introduce an important piece of information for the rational design of devices based on electron transfer between metal and biological systems.

Experimental Section

The redox polymer $[Os(bpy)_2ClpyNH]$–poly(allylamine) (OsPA) was synthesized as previously reported.[29] The stoichiometry ratio between the osmium complex and the allylamine monomer was 1:35. AuNPs with a diameter of 11 ± 3 nm were synthesized according to a published procedure.[30] Raman experiments were conducted on bulk gold electrodes. SPR measurements were performed on high quality glass slides coated with 50 nm of gold and 5 nm of chromium as an adhesion layer (BioNavis Ltd). Gold-coated quartz crystals (14 mm diameter) with a fundamental resonance frequency of 5 MHz (QSX 301, Q-sense AB) were used for QCM-D experiments. Electrochemical experiments were conducted on gold-coated silicon substrates.

Preparation of polyelectrolyte-surfactant composite material (OsPA-DS)

Sodium dodecylsulfate (SDS, 200 μL, 1%) in Milli-Q water was added to OsPA (100 μL, 0.2 mM). The mixture immediately generated a precipitate (OsPA-DS), which was easily separated by centrifugation. The OsPA-DS complex was analyzed by elementary microanalysis showing a dodecylsulfate to allylamine ratio of approximately 1:1 (calculated as N/S ratio). The precipitate was dissolved in 250 μL of dimethylformamide (DMF) and sonicated for 15 min to facilitate complete dissolution of the solid. The final solution was used for substrate modification. Osmium charges were determined by anodic peak integration in cyclic voltammetries at different scan rates and averaging the results.

Preparation of polyelectrolyte-surfactant-AuNP composite material (OsPA-DS-AuNP)

A AuNP suspension (2 mL) was centrifuged at 3000 rpm for 60 min. The resulting pellet was re-suspended with DMF (50 μL) and sonicated for 30 min to obtain a well-dispersed suspension. 100 μL of the DMF solution of OsPA-DS previously described was then added to the AuNP suspension and sonicated for 30 min to give a homogeneous dispersion. The final dispersion was used for substrate modification. Osmium charges were determined by anodic peak integration of cyclic voltammetries at different scan rates and averaging the results.

Substrate modification

In all the experiments, the substrate was gold with the exception of GISAXS in which silicon was used. Substrates were modified by the same experimental procedure. The first step consisted of the application by spin coating a uniform layer of the corresponding DMF solution previously described. Afterwards, the substrates were left at room temperature for 2 h to allow complete evaporation of the solvent. Then, they were rinsed with Milli-Q water and dried under a stream of nitrogen gas. For the same substrate and solution, different thicknesses could be obtained by applying different numbers of coats.

Resonance Raman spectroelectrochemistry

Resonance Raman (RR) spectra were measured in backscattering geometry using the 514 nm line of an Ar ion laser (Coherent Innova 70C, USA) focused onto the electrode surface.[31] The spectroelectrochemical cell was equipped with an Au working electrode, a Pt-wire counter electrode, and an Ag/AgCl reference electrode. After polynomial background subtraction, RR spectra were subjected to band-fitting analysis using home-made software. The total area of the fitted peaks between 1150 and 1600 cm^{-1} was employed for connectivity calculations.

Atomic force microscopy

Tapping mode™ AFM was performed by using a Nanoscope IIIa-Quadrex Multimode AFM (Bruker, Santa Barbara, CA, USA) equipped with a vertical J-scanner, having a maximal lateral range of approximately 150 μm. Topographic (height) and phase imaging were recorded simultaneously under dry nitrogen by using silicon probes. The scan rate was 1 Hz and each sample was imaged several times at different locations on the substrate to ensure reproducibility. Measurements of roughness were made in the NanoScope off-line software, NanoScope 5.30r3sr3 (Bruker Nano Inc.).

Surface plasmon resonance spectroscopy

Multi-parametric surface plasmon resonance (MP-SPR) experiments were carried out by using a SPR Navi 210A instrument (BioNavis Ltd, Tampere, Finland). All experiments were performed in a 0.1 M

Tris-HCl, 0.1 M NaCl buffer solution at pH 7.4. The flow rate used in the experiments was 20 $\mu L\,min^{-1}$ and the temperature was 27 °C. The measurements were performed at 670 nm in the angular scan mode. After a stable baseline was obtained, 1 $mg\,mL^{-1}$ GOx solution was allowed to flow and the adsorption was monitored in situ; the sample contact time was 10 min. Then, the system was rinsed for 20 min with the carrier buffer.

Quartz-crystal microbalance with dissipation monitoring (QCM-D)

The QCM-D experiments were performed by using a Q-Sense E1 (Biolin Scientific, Sweden) equipped with a Flow Module. For all measurements, QSX 301 gold sensors were used. Measurements were recorded at several odd overtones and frequency shifts were normalized by division with the overtone number. All experiments were performed in a 0.1 M Tris-HCl, 0.1 M NaCl buffer solution at pH 7.4; the flow rate used in the experiments was 150 $\mu L\,min^{-1}$, at 27 °C. After a stable baseline was obtained, a 1 $mg\,mL^{-1}$ GOx solution was allowed to flow through the system and the GOx adsorption was performed; the sample contact time was 40 min and the rinsing time after GOx injection was 20 min.

Grazing-incidence small-angle X-ray scattering (GISAXS)

GISAXS measurements were performed at the D10AXRD2 beamline of Laboratório Nacional de Luz Síncrotron (LNLS) (Campinas, Brazil) ($\lambda = 1.608$ Å). The sample-to-detector distance was kept at 550 mm, the outgoing photons were detected by using a PILATUS 100 K detector (DECTRIS AG, Switzerland). Sample temperature was kept at 20 °C and sample humidity was controlled by using a home-built chamber.

Electrochemical measurements

Cyclic voltammetry experiments were carried out by using a Teq-02 potentiostat (TEQ, Argentina) using a three-electrode Teflon electrochemical cell equipped with a platinum mesh counter electrode and an Ag/AgCl reference electrode. Unless otherwise stated, all electrochemical experiments were performed at room temperature (22 °C) in a 0.1 M Tris-HCl, 0.1 M NaCl buffer solution at pH 7.4.

Acknowledgments

The authors acknowledge financial support from Universidad de Buenos Aires (X0513), ANPCyT (PICT 2011–0406, PICT 2010–2554, PICT 2010–457, PICT 2010–70, and PPL 2011–003), Centro Interdisciplinario de Nanociencia y Nanotecnología (CINN-ANPCyT-Argentina), and the Max-Planck-Gesellschaft (Max Planck Partner Group for Functional Supramolecular Bioconjugates, INIFTA/MPIP). O.A. and M.C. gratefully acknowledge the Laboratório Nacional de Luz Síncrotron (LNLS, Campinas - Brazil) for financial support and granting access to synchrotron facilities (XRD2–13391, XRD2–11639, XRD2–14358, and SXS–11642). M.L.C. acknowledges CONICET for a postdoctoral fellowship. W.M., D.P., L.I.P., D.H.M., M.C., O.A., and F.B. are CONICET fellows.

Keywords: electron transfer · glucose catalysis · glucose oxidase · gold nanoparticles · mesostructure · redox polyelectrolyte

[1] J. Wang, *Chem. Rev.* **2008**, *108*, 814–825.
[2] S. Carrara, S. Ghoreishizadeh, J. Olivo, I. Taurino, C. Baj-Rossi, A. Cavallini, M. Op de Beeck, C. Dehollain, W. Burleson, F. G. Moussy, A. Guiseppi-Elie, G. De Micheli, *Sensors* **2012**, *12*, 11013–11060.
[3] W. Putzbach, N. J. Ronkainen, *Sensors* **2013**, *13*, 4811–4840.
[4] A. K. Baba, P. Taranekar, R. R. Ponnapati, W. Knol, R. C. Advincula, *ACS Appl. Mater. Interfaces* **2010**, *2*, 2347–2354.
[5] a) F. Lisdat, R. Dronov, H. Möhwald, F. W. Scheller, D. G. Kurth, *Chem. Commun.* **2009**, 274–283; b) D. Pallarola, N. Queralto, W. Knoll, M. Ceolín, O. Azzaroni, F. Battaglini, *Langmuir* **2010**, *26*, 13684–13696; c) D. Pallarola, N. Queralto, W. Knoll, O. Azzaroni, F. Battaglini, *Chem. Eur. J.* **2010**, *16*, 13970–13975; d) D. Pallarola, C. von Bildering, L. I. Pietrasanta, N. Queralto, W. Knoll, F. Battaglini, O. Azzaroni, *Phys. Chem. Chem. Phys.* **2012**, *14*, 11027–11039.
[6] a) A. Heller, B. Feldman, *Acc. Chem. Res.* **2010**, *43*, 963–973; b) A. Heller, *Acc. Chem. Res.* **1990**, *23*, 128–134.
[7] S. C. Feifel, A. Kapp, R. Ludwig, L. Gorton, F. Lisdat, *RSC Adv.* **2013**, *3*, 3428–3437.
[8] a) Y. Yu, Z. Chen, S. He, B. Zhang, X. Li, M. Yao, *Biosens. Bioelectron.* **2014**, *52*, 147–152; b) Y. Zhang, C. Xu, B. Li, Y. Li, *Biosens. Bioelectron.* **2013**, *43*, 205–210; c) P. R. Dalmasso, M. L. Pedano, G. A. Rivas, *Biosens. Bioelectron.* **2013**, *39*, 76–81; d) G. A. Rivas, M. D. Rubianes, M. C. Rodríguez, N. F. Ferreyra, G. L. Luque, M. L. Pedano, S. A. Miscoria, C. Parrado, *Talanta* **2007**, *74*, 291–307; e) A. Trifonov, K. Herkendell, R. Tel-Vered, O. Yehezkeli, M. Woerner, I. Willner, *ACS Nano* **2013**, *7*, 11358–11368.
[9] a) E. Katz, I. Willner, J. Wang, *Electroanalysis* **2004**, *16*, 19–44; b) E. Katz, I. Willner, *Angew. Chem.* **2004**, *116*, 6166–6235; *Angew. Chem. Int. Ed.* **2004**, *43*, 6042–6108; c) Y. Xiao, F. Patolsky, E. Katz, J. F. Hainfeld, I. Willner, *Science* **2003**, *299*, 1877–1881; d) O. Yehezkeli, Y.-M. Yan, I. Baravik, R. Tel-Vered, I. Willner, *Chem. Eur. J.* **2009**, *15*, 2674–2679; e) O. Yehezkeli, R. Tel-Vered, S. Raichlin, I. Willner, *ACS Nano* **2011**, *5*, 2385–2391.
[10] a) K. Saha, S. S. Agasti, C. Kim, X. Li, V. M. Rotello, *Chem. Rev.* **2012**, *112*, 2739–2779; b) A. Walcarius, S. D. Minteer, J. Wang, Y. Lin, A. Merkoçi, *J. Mater. Chem. B* **2013**, *1*, 4878–4908; c) A. Merkoçi, *Electroanalysis* **2013**, *25*, 15–27.
[11] a) B. Haghighi, M. A. Tabrizi, *Colloids Surf. B* **2013**, *103*, 566–571; b) S. Lee, B. S. Ringstrand, D. A. Stone, M. A. Firestone, *ACS Appl. Mater. Interfaces* **2012**, *4*, 2311–2317; c) C. Suna, X. Chena, A. Hana, Q. Zhouc, C. Maoa, Q. Zhua, J. Shen, *Anal. Chim. Acta* **2013**, *776*, 17–23.
[12] M. N. Zafar, X. Wang, C. Sygmund, R. Ludwig, D. Leech, L. Gorton, *Anal. Chem.* **2012**, *84*, 334–341.
[13] a) J. F. Hicks, Y. Seok-Shon, R. W. Murray, *Langmuir* **2002**, *18*, 2288–2294; b) C. R. Bradbury, J. Zhao, D. J. Fermin, *J. Phys. Chem. C* **2008**, *112*, 10153–10160; c) A. R. Schmidt, N. D. T. Nguyen, M. C. Leopold, *Langmuir* **2013**, *29*, 4574–4583; d) C. Ou, R. Yuan, Y. Chai, R. Tang Chai, X. He, *Anal. Chim. Acta* **2007**, *603*, 205–213.
[14] G. Decher, in *Multilayer Thin Films* (Eds.: G. Decher, J. B. Schlenoff), Wiley-VCH, Weinheim, **2002**, Ch. 1, pp. 1–46.
[15] a) C. F. J. Faul, M. Antonietti, *Adv. Mater.* **2003**, *15*, 673; b) O. Ikkala, G. Ten Brinke, *Science* **2002**, *295*, 2407; c) A. F. Thünemann, *Prog. Polym. Sci.* **2002**, *27*, 1473.
[16] a) A. Perico, A. Ciferri, *Chem. Eur. J.* **2009**, *15*, 6312; b) F. Gröhn, *Macromol. Chem. Phys.* **2008**, *209*, 2291; c) M. Antonietti, J. Conrad, A. Thünemann, *Macromolecules* **1994**, *27*, 6007–6011; d) S. Zhou, C. Burger, B. Chu, *J. Phys. Chem. B* **2004**, *108*, 10819–10824; e) A. F. Thünemann, M. Müller, H. Dautzenberg, J. F. Joanny, H. Löwen, *Adv. Polym. Sci.* **2004**, *166*, 113.
[17] M. L. Cortéz, G. A. González, F. Battaglini, *Electroanalysis* **2011**, *23*, 156–160.
[18] a) M. L. Cortez, D. Pallarola, M. Ceolín, O. Azzaroni, F. Battaglini, *Anal. Chem.* **2013**, *85*, 2414–2422; b) M. L. Cortez, D. Pallarola, M. Ceolín, O. Azzaroni, F. Battaglini, *Chem. Commun.* **2012**, *48*, 10868–10870.
[19] a) M. L. Cortez, M. Ceolín, O. Azzaroni F., Battaglini, *Anal. Chem.* **2011**, *83*, 8011–8018; b) A. S. Peinetti, L. P. Méndez De Leo, G. A. González, F. Battaglini, *J. Colloid Interface Sci.* **2012**, *386*, 44–50.
[20] R. W. Murray, *Chem. Rev.* **2008**, *108*, 2688–2720.
[21] a) N. M. O'Boyle, T. Albrecht, D. H. Murgida, L. Cassidy, J. Ulstrup, J. Vos, *Inorg. Chem.* **2007**, *46*, 117–124; b) N. Tognalli, A. Fainstein, C. Bonazzola, E. J. Calvo, *J. Chem. Phys.* **2004**, *120*, 1905–1911.
[22] P. N. Bartlett, K. F. E. Pratt, *J. Electroanal. Chem.* **1995**, *397*, 61–78.

[23] F. Höök, B. Kasemo, T. Nylander, C. Fant, K. Sott, H. Elwing, *Anal. Chem.* **2001**, *73*, 5796 – 5804.
[24] M. Rodahl, F. Höök, C. Fredriksson, C. A. Keller, A. Krozer, P. Brzezinski, V. Voinova, B. Kasemo, *Faraday Discuss.* **1997**, *107*, 229 – 246.
[25] X.-y. Chen, J.-r. Li, X.-c. Li, J. Jiang, *Biochem. Biophys. Res. Commun.* **1998**, *245*, 352 – 355.
[26] Z. J. Chen, X. M. Ou, F. Q. Tang, L. Jiang, *Colloids Surf. B* **1996**, ***7***, 173 – 179.
[27] J. N. Chazalviel, P. Allongue, *J. Am. Chem. Soc.* **2011**, *133*, 762 – 764.
[28] A. Barfidokht, S. Ciampi, E. Luais, N. Darwish, J. J. Gooding, *Anal. Chem.* **2013**, *85*, 1073 – 1080.
[29] C. Danilowicz, E. Cortón, F. Battaglini, *J. Electroanal. Chem.* **1998**, *445*, 89 – 94.
[30] C. J. Kiely, J. Fink„ M. Brust, D. Bethell, D. J. Schiffrin, *Nature* **1998**, *396*, 444 – 446.
[31] J. Hrabakova, K. Ataka, J. Heberle, P. Hildebrandt, D. H. Murgida, *Phys. Chem. Chem. Phys.* **2006**, *8*, 759 – 766.

Received: March 21, 2014
Published online on August 29, 2014